The ALICE Transition Radiation Detector

C. Lippmann for the ALICE collaboration
Gesellschaft für Schwerionenforschung mbH, Darmstadt, Germany

The Transition Radiation Detector is one of the main detector components of the ALICE experiment at the LHC. It increases the tracking performance of the ALICE central barrel detectors and provides separation of electrons from the large background of pions. By combining these two functions, the TRD also provides a fast trigger on high transverse momentum electrons. In this publication, the TRD system is described in detail.

1. Introduction

The Large Hadron Collider (LHC) is the new accelerator currently constructed at CERN in Geneva, Switzerland. From the year 2007 on it will provide collisions of protons at very high energies ($\sqrt{s} = 14\,\mathrm{TeV}$) and luminosities ($\mathcal{L} = 10^{34}\,\frac{1}{\mathrm{cm^2\,s}}$). In addition, it will provide collisions of lead nuclei at centre-of-mass energies of 5.5 TeV per nucleon pair and maximum luminosity $\mathcal{L} = 10^{27}\,\frac{1}{\mathrm{cm^2\,s}}$. ALICE (A Large Ion Collider Experiment) is the dedicated heavy ion experiment at the LHC [1]. Its aim is to study the physics of strongly interacting matter at extreme energy densities. As probes of the plasma of quarks and gluons, that will be produced in these collisions, quarkonia (J/Ψ, Ψ', Υ, ...), open charm and open beauty, as well as jets can be used. Quarkonia are reconstructed via their decays into dielectron pairs (e^+ e^-), which carry rather large transverse momenta ($p_T \gtrsim 1.5\,\mathrm{GeV/c}$), leading to almost straight tracks in the field of the ALICE L3 magnet.

Fig. 1 shows a simulated event with only high transverse momentum tracks ($p_T > 1.5\,\mathrm{GeV/c}$). The search for these tracks is a challenging task in the high densities of charged particle tracks encountered in heavy ion collisions (At the LHC the estimated maximum multiplicity per unit of rapidity is $dN_{ch}/dy \leq 8\,000$ at mid-rapidity.). This is especially true, if a fast trigger decision is to be given: Then the up to 16 000 charged particle tracks have to be all reconstructed three dimensionally in a very short time in order to find high-p_T tracks. In ALICE a Transition Radiation Detector [2] (TRD) was added to perform that task. In order to separate electrons from the background of high-p_T pion tracks in the momentum range of interest for the TRD ($1 < p < 10\,\mathrm{GeV/c}$), the different ionization energy loss of electrons and pions and the production of transition radiation (TR) are used.

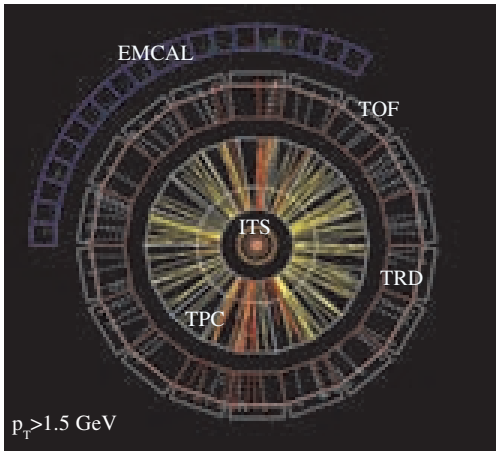

Figure 1: Simulated event (AliRoot) showing only tracks with high transverse momentum ($p_T > 1.5\,\mathrm{GeV/c}$) in the Inner Tracking System (ITS), Time Projection Chamber (TPC), Transition Radiation Detector (TRD), Time Of Flight System (TOF) and the Electromagnetic Calorimeter (EMCAL).

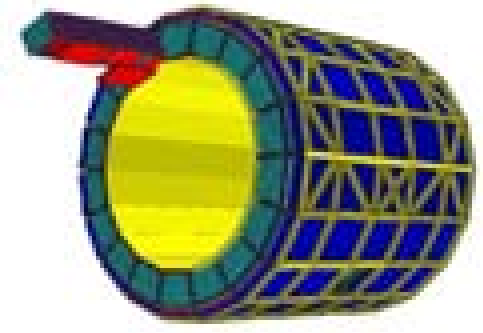

Figure 2: Drawing of the 18 TRD supermodules that surround the ALICE TPC. One supermodule is shifted longitudinally to show that it contains the TRD drift chambers. One drift chamber is again shifted to demonstrate its size. The whole TRD consists of 540 drift chambers. Its diameter and length are both about 7 m.

2. TRD Working Principle

The TRD surrounds the large TPC (Time Projection Chamber) in the central barrel of ALICE. It consists of 540 large area drift chambers with the drift direction perpendicular to the wire planes, and with 1.18 million readout channels. The size of the drift chambers is $\approx 1.2 \times 1.4\,\mathrm{m}^2$; they are arranged in 18 *supermodules* containing 5 longitudinal stacks and 6 radial layers each (See Fig. 2).

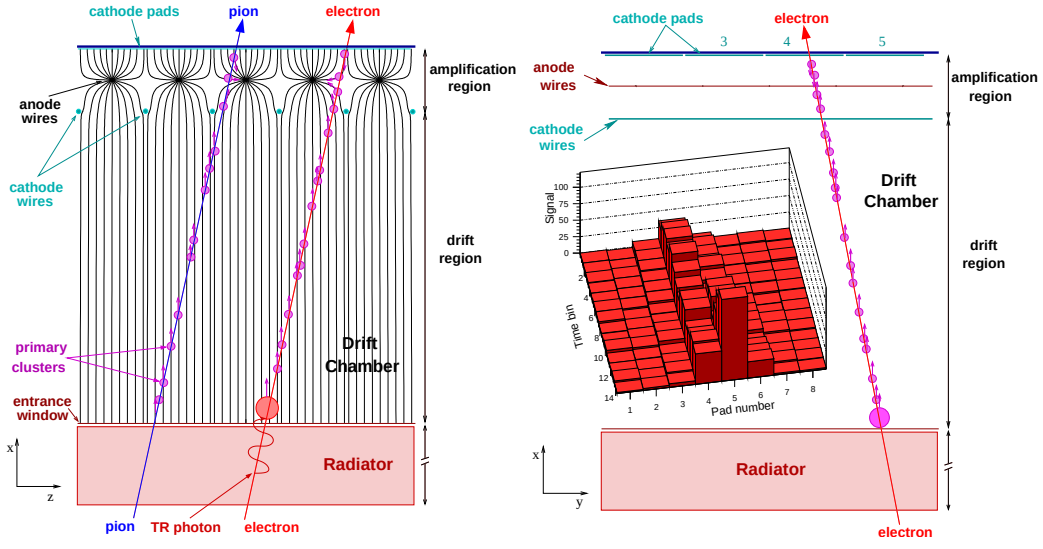

Figure 3: Schematic illustration of the TRD principle. The left panel shows a projection in the plane perpendicular to the wires. Electrons produced by ionization energy loss ($\mathrm{d}E/\mathrm{d}x$) and by TR absorption drift along the field lines towards the anode wires. The right panel shows a projection in the bending plane of the ALICE magnetic field. In this direction the cathode plane is segmented into pads from 0.635 to 0.785 cm width. The insert shows for a measured electron track the distribution of pulse height over pads and time bins spanning the drift region. The radiator is not to scale.

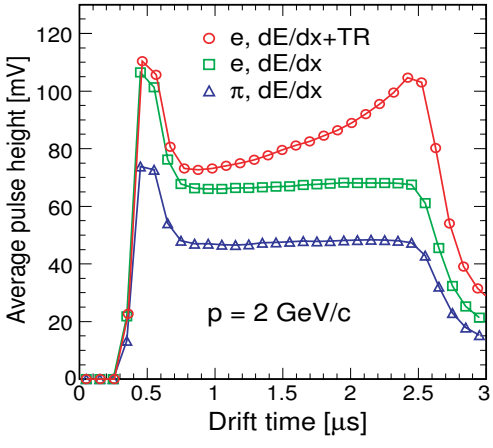

Figure 4: Average pulse height as function of the drift time.

Transition radiation (TR) is produced by fast ($\gamma \gtrsim 1\,000$) particles at the crossing of boundaries between materials with different dielectric constants. In the momentum range from 1 to 10 GeV/c only electrons produce TR. The production probability is about 1 % per boundary crossing, thus several hundred interfaces are used in practical TR detectors. Taking into account absorption inside the radiator itself, a radiator of about 100 foils produces about one net TR photon with energy in the useful range of soft X-rays (1 to 30 keV). In the ALICE TRD a sandwich radiator made of foam and fiber materials is used, since this structure can also provide mechanical rigidity against the deformations caused by gas overpressure.

Schematic cross sections of a TRD drift chamber are shown in Fig. 3. The width of the amplification region is 0.7 cm, the width of the drift region is 3 cm and the thickness of the radiator is 4.8 cm. For pions only ionization clusters are produced in the gas, while for electrons TR energy is deposited on top. A heavy gas mixture based on Xenon is used to provide efficient TR photon absorption; 15 % CO_2 is added as a quencher.

The free electrons produced by ionization and TR absorption drift towards the anode wires where they create avalanches. The drift chambers are operated at low gas gain to avoid space charge effects [3]. The signals induced on the cathode pads ($\approx 0.75 \times 8\,\mathrm{cm}^2$) are read out at 10 MHz such that the signal height on all pads can be sampled in time bins of 100 ns width. Due to the drift velocity in the drift region of 1.5 $\frac{\mathrm{cm}}{\mu\mathrm{s}}$ a time bin corresponds to a space interval of 1.5 mm in drift direction. A second coordinate (the direction running parallel to the wires) can be reconstructed by charge sharing on adjacent cathode pads, such that tracking in the bending plane becomes possible.

Fig. 4 shows average signals [4] for electrons and pions. The different pulse heights indicate the different ionization energy loss of the two particles, while the characteristic peak at larger drift times in case of electrons is due to absorbed TR.

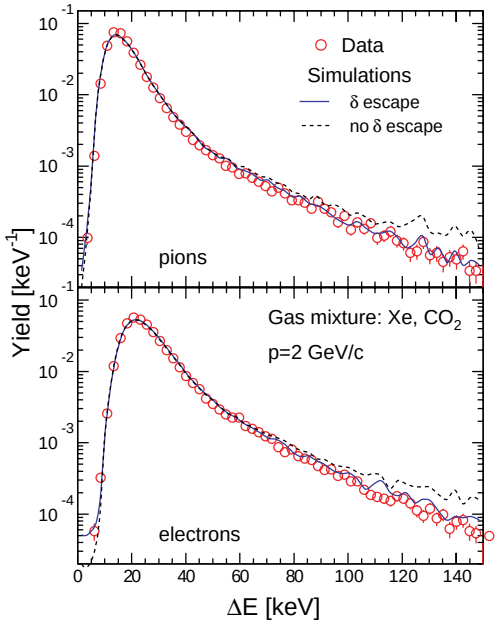

Figure 5: Measured $\mathrm{d}E/\mathrm{d}x$ spectra for pions (top panel) and electrons (bottom panel) at a momentum of 2 GeV/c together with simulations (lines).

3. Electron Identification with the TRD

For the TRD a pion rejection factor of about 100 at an electron efficiency of 90 % is required. The use of a *Likelihood method* requires the availability of probability distributions to be an electron and to be a pion for all momenta. In our case these distributions are defined by the spectra of deposited energy for these particles. Thus a very detailed understanding of the spectral distributions of $\mathrm{d}E/\mathrm{d}x$ and TR is needed.

3.1. dE/dx

Fig. 5 shows measured $\mathrm{d}E/\mathrm{d}x$ spectra for pions and electrons at a momentum of 2 GeV/c. The inclusion of the escape of high energy delta electrons in the simulations leads to a very good agreement. This is also true for the performance as function of momentum, which is not shown here [5].

3.2. TR

Spectral distributions of the energy of TR photons were measured using a method demonstrated in [6]. Our setup and measurements are described in detail in [7]. We used a small prototype drift chamber, where the radiator was detached from the drift volume, which was then only closed by a thin aluminized mylar foil. A magnet was used to deflect the beam such that the TR photons were well separated from the $\mathrm{d}E/\mathrm{d}x$ from the particle tracks. An example event

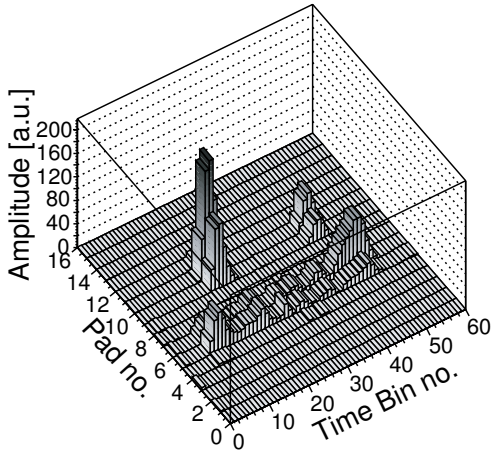

Figure 6: Pulse height versus drift time on sixteen adjacent cathode pads for an example event. The ionization signal by a beam electron and two well separated photon clusters are clearly visible.

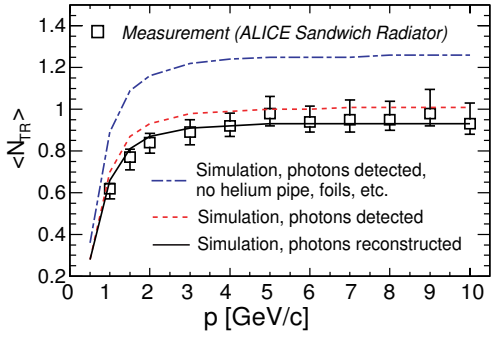

Figure 7: Measured and simulated dependence of the mean number of detected TR photons $\langle N_{TR} \rangle$ on the momentum. The simulated data show the mean number of TR photons absorbed in the drift chamber for two cases: With and without the additional material from the beam setup (helium pipe, entrance windows and some air) included in the simulation. In addition, the mean number of photons reconstructed by the TR cluster search algorithm is shown.

is shown in Fig. 6. In order to minimize absorption of the TR photons before the drift chamber, a pipe filled with helium was used. The sampling frequency was increased in order to arrive at a time bin size of 50 ns and thus a better TR cluster separation in drift direction.

Fig. 7 shows the average number of TR photons detected for all measured momenta. The onset of TR is visible around 0.5 GeV/c; above 3 GeV/c the TR yield saturates. The simulations show that the helium pipe and entrance windows absorb about 0.3 photons. They also point out the limitations of the algorithm that was used to search TR photons in the data, namely its limited efficiency to separate very close TR clusters.

Fig. 8 shows measured and simulated spectra of

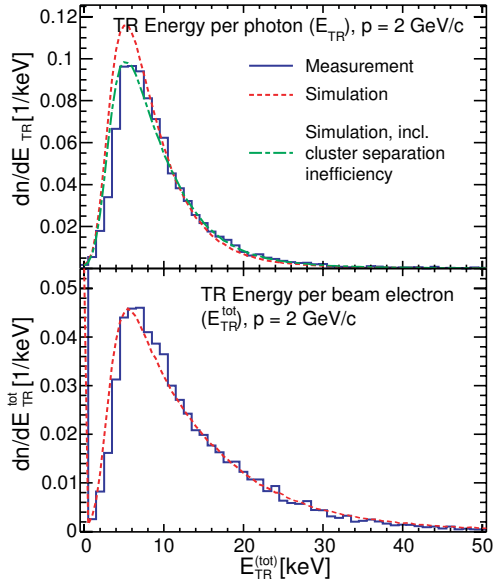

Figure 8: Measured and simulated TR spectra at 2 GeV/c. The upper panel shows the distribution of the energy for single TR photons. The lower panel shows the distribution of the total TR energy detected per incident beam electron. Here, the entries at 0 keV (off scale) correspond to events when no photon was detected.

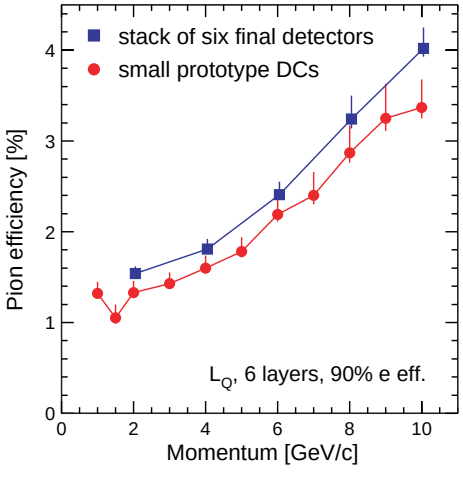

Figure 9: Measured electron identification performance.

pure TR. A simulation procedure for regular foil radiators [6] was used; in order to reproduce our measurements with an irregular radiator we parameterize the radiator. In general, a simulation using the theory for irregular radiators would be preferable and is presently under investigation.

The measured electron identification performance for the small prototype drift chambers and for a stack of six final, real-sized TRD chambers is shown in Fig. 9. The chambers in the stack performed a bit worse due to a noise problem. However, we reach a pion rejection factor (inverse of pion efficiency) of around

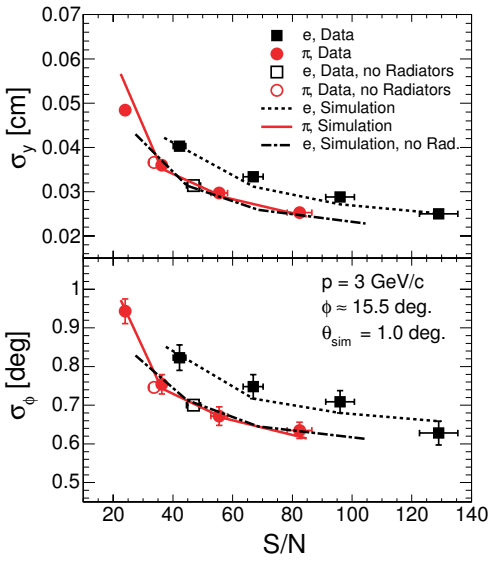

Figure 10: Position resolution (upper panel, σ_y) and angular resolution (lower panel, σ_ϕ) as a function of the signal-to-noise ratio (S/N). The filled squares (circles) show the measured data for electrons (pions) with radiators in front of the drift chambers. The open squares (circles) show the measured data for electrons (pions) with no radiators for one S/N value. The lines show simulation results with and without TR [10].

100 at 90 % electron efficiency. Further improvement can be achieved with the L_{QX} method, where the position of the largest energy deposit (TR photons are preferably absorbed close to the drift cathode, see Fig. 4) is also analyzed [8], and with a neural network algorithm [9].

4. Tracking with the TRD

The TRD should be capable of finding stiff particle tracks (fast stand-alone tracking, TRD trigger). Here a momentum resolution (at $1 < p_T < 10$ GeV/c) of $\frac{\Delta p_T}{p_T} \approx 5\,\%$ is sufficient. In addition, the TRD should also increase the tracking capability of the ALICE barrel detectors. This requires that the tracks reconstructed in the six TRD layers and in the TPC need to be matched. This mainly drives the tracking requirements for the TRD. In the bending plane of the magnetic field this translates to:

1. a hit resolution of $\sigma_y \lesssim 400\,\mu$m (for each time bin) and

2. an angular resolution of $\sigma_\phi \lesssim 1°$ (for each TRD layer).

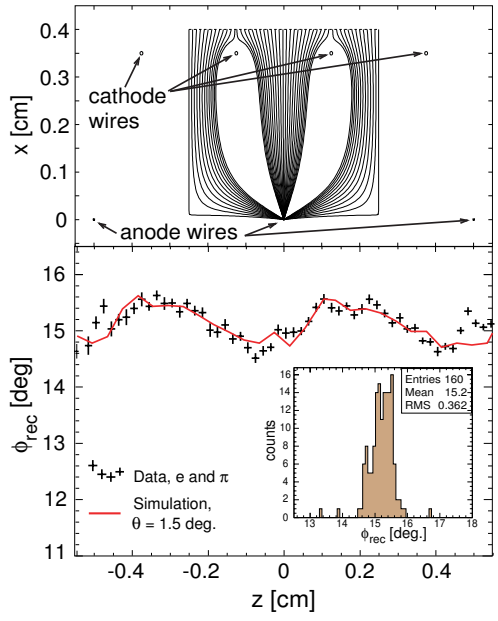

Figure 11: Upper panel: Ideal drift lines for electrons coming from the drift region at different positions with respect to the coordinate across the wires (z). The anode wire plane is at $x = 0\,\text{cm}$; the cathode wire plane is at $x = 0.35\,\text{cm}$. Lower panel: Systematic variation of the reconstructed angle ϕ_{rec} with the z-coordinate. We show measurements (symbols) and simulated results (line). The insert shows a projection of the measured data on the ordinate, giving the overall effect due to non-linearity [10].

4.1. Position Reconstruction

The dependence of σ_y and σ_ϕ on the signal-to-noise value is shown in Fig. 10. The incident angle of the beam was $\phi \approx 15\,^\circ$; the measured data are nicely reproduced by the simulations. The measured data for pions and electrons with TR lie on two separate curves, roughly of $1/\sqrt{S/N}$ form. At a given S/N value, the resolution is worse for electrons as compared to pions. The data without radiators show better resolutions for electrons and lie on the same curve as the pion data, while for pions the performance is similar with and without radiators. The processes related to the TR absorption turn out to cause a significant deterioration of the detector resolution for electrons. L-shell fluorescence photons are commonly produced and carry energies around 5 keV; their absorption length is about 4 mm in Xenon. Their influence on the resolution is dominant, while the influence of photoelectrons, Auger electrons, K- and M-shell fluorescence photons is small [10].

4.2. Nonlinearities

The lower panel of Fig. 11 shows the systematic variation of the reconstructed angle ϕ_{rec} with the coordinate across the wires. Clearly visible is the influence of the anode wire grid with 0.5 cm periodicity. This systematic effect can be approximately reproduced by the simulation and is explained by nonlinearities in the time-space relationship. A small variation of the angle θ from zero has to be assumed, for $\theta = 0\,^\circ$ the systematic effect disappears [10].

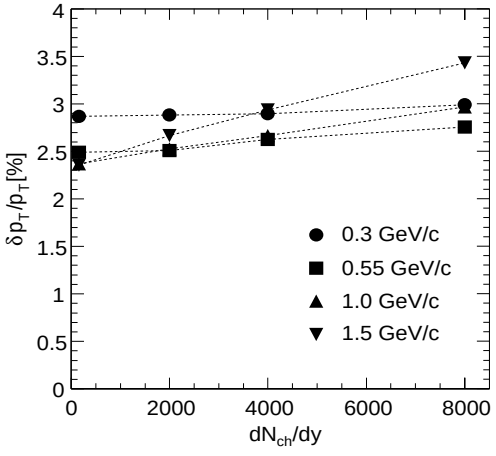

Figure 12: Simulated momentum resolution of the TRD for pion tracks at different transverse momenta as a function of the multiplicity [2].

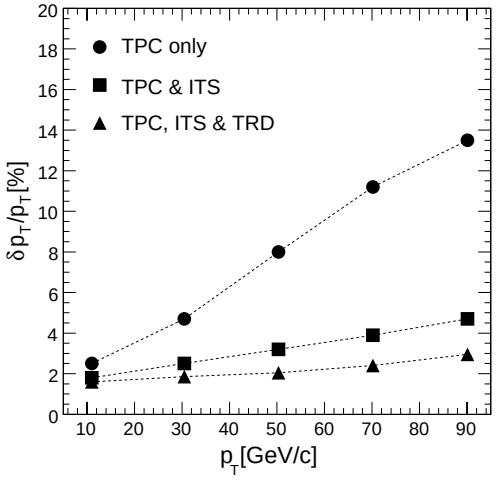

Figure 13: Simulated momentum resolution of the ALICE barrel detectors in different combinations.

4.3. Standalone TRD Tracking Performance

At the trigger level a good momentum resolution (TRD only) leads to a sharper threshold and a smaller probability of fake tracks, but the requirements are not strict. As shown in Fig. 12, the TRD will provide a momentum resolution below 4 % at all multiplicities up to the maximum expected multiplicity of $dN_{ch}/dy = 8\,000$.

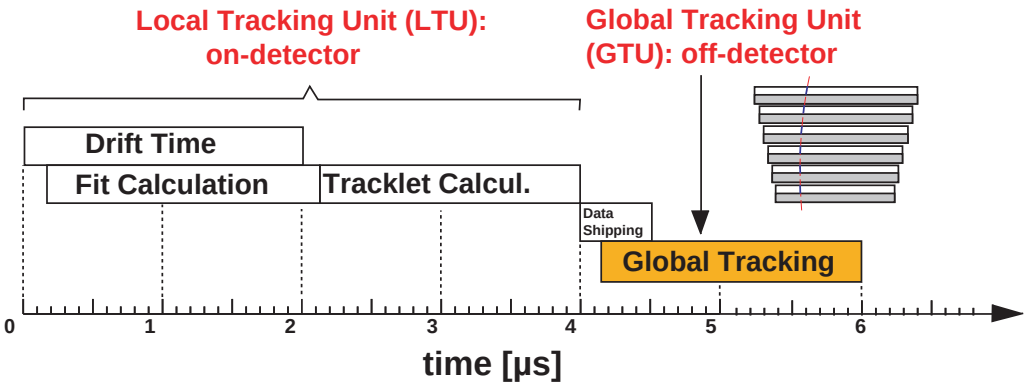

Figure 14: Time sequence for the TRD trigger.

4.4. Global Tracking Performance

The transverse momentum resolution requirements of the ALICE central barrel are fulfilled already by just combining the TPC and ITS. The main function which the TRD needs to fulfill is electron identification. Nevertheless, including the TRD in the global tracking improves the momentum resolution to be below 3 % for momenta up to 90 GeV/c (See Fig. 13).

5. Triggering with the TRD

The requirement for the TRD trigger is a latency of 6.1 μs. This very tight time budget has to be sufficient for the digitization and data processing in all TRD channels. The tracks of all of the up to 16 000 charged primary particles (at the maximum expected multiplicity) crossing the TRD need to be reconstructed in order to find high-p_T electron candidates [2, 11, 12].

The strategy is shown schematically in Fig. 14. Local Tracking Units (LTU) preprocess the data and apply pattern matching algorithms in application-specific chips directly on the drift chambers. Linear tracklet fits are performed after completion of the electron drift, when all information is available, and high-p_T tracklet candidates can be selected by means of maximum deflection compared to that expected from straight trajectories. A tracklet denotes a short track segment found in a single TRD layer.

The LTUs send their high-p_T tracklet candidates together with their particle identification (PID) information—based on the total energy loss and the depth profile of the deposited energy—to the Global Tracking Unit (GTU). The time budget for this step is 600 ns. The GTU reassembles the resulting track segments of different drift chambers three-dimensionally. From the curvature of the reconstructed tracks, the momentum of the originating particle is calculated. The global PID information is calculated combining the local PID measures to finally make the trigger decision. This part of the online processing must be completed in less than 2 μs.

5.1. Multi Chip Modules

The overall TRD electronics chain is sketched in Fig. 15. The LTUs are realized by highly integrated, full custom front-end electronics. An 18 channel analog preamplifier and shaper (PASA[1]) and a mixed-signal chip performing event buffering and local tracking (TRAP[2] [13]) are combined on Multi-Chip Modules (MCM), designed as ball grid arrays which are directly soldered to the detectors readout board PCBs. The TRAP chip contains 21 low power ADCs[3], and digital filters [14], which perform the required nonlinearity, baseline and gain corrections, as well as signal symmetrization (cancellation of the ion tail of the drift chamber signals) and crosstalk suppression. The preprocessor contains hit detection and hit selection, calculates the position (using the pad response), detects tracklets and calculates their fit parameters in four arithmetic units. The tracklet processor with four CPUs identifies high-p_T track candidates for further processing. An 8 Bit 120 MHz double data rate network interface performs the readout on each drift chamber, merging its own data and that of neighboring TRAP chips into a common data stream. Each MCM processes 18 channels. The additional channels in the ADC are used only for position calculation using the pad response. 16 signal processing MCMs

[1] The PASA has 120 ns shaping time, an equivalent noise charge of 850 electrons at 25 pC, a gain of 12.4 mV/fC, an integral nonlinearity of 0.3 % and a power consumption of 12 mW/channel. It is realized in AMS 0.35 μm technology and occupies 21.3 mm^2 of silicon.

[2] The TRAP chip is an ASIC in CMOS 0.18 μm technology.

[3] The ADC digitizes the analog data at 10 MHz and has an effective number of bits of 9.5. It consumes about 12.5 mW/channel and occupies 0.11 mm^2 of silicon.

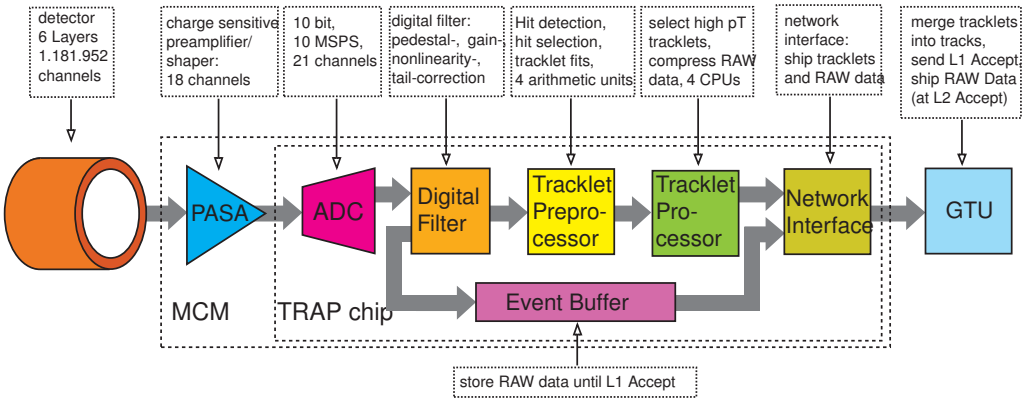

Figure 15: Overview of the TRD electronics chain.

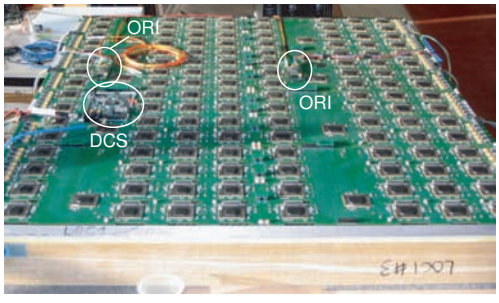

Figure 16: 8 readout boards, 2 Optical Readout Interfaces (ORI) and a Detector Control System (DCS) board on a TRD drift chamber.

and 1 or 2 data collecting MCMs are implemented on each readout board. Due to this high density of electronics and the need to maximize active detector area all electronics has to be located in the active area. An image of a TRD drift chamber completely covered with readout electronics is shown in Fig. 16. Here, a noise on-detector of about 1.150 electrons is achieved on average.

5.2. Optical Readout and GTU

The high-speed TRD readout is performed with 1 080 Optical Readout Interfaces (ORI) providing 2.5 GBit/s optical links (2 per drift chamber). It is done in two stages: During the trigger processing all tracklet candidates are shipped within 600 ns from the 65 664 MCMs to the global tracking unit (GTU) for merging of the tracklets. The GTU processes up to 20 000 track segments per event in about 1.4 μs by means of massive parallelism. 90 independent Track Matching Units (TMU) with a large FPGA search for global high-p_T tracks ($p_T > 3$ GeV/c). Each TMU receives data from one detector stack with 6 drift chamber layers each via 12 links. Later, in case of an accept decision, the GTU also receives the entire RAW data from the on-detector event buffers and stores the event in a multi-event buffer for later readout in case of a Level 2 Accept.

5.3. Detector Control System

The readout electronics on one TRD drift chamber is controlled by dedicated Detector Control System boards (DCS). It contains an FPGA and an ARM core running the Linux operating system. The DCS boards control the voltage regulator shutdown on the readout boards, configure all of the up to 138 MCMs on a drift chamber and distribute clock and trigger signals.

6. TRD Gas System

The requirements for the TRD gas system are driven by the high price of the used Xe gas and by the geometrical stability of the rather large drift chambers against deformations caused by pressure differences. The gas has to be recirculated in a closed loop system and purified. Moreover, the working overpressure has to be limited to below 1 mbar.

The total gas volume of all drift chambers is about 27.2 m^3 and the height span from the lowest to the highest drift chamber is about 7 m. As a consequence of the heavy gas mixture, a pressure difference of 2.5 mbar would be present already due to the Xe hydrostatic pressure. To overcome this problem, the gas system is segmented into 14 height sections. Thin gas pipes are used between the distribution module—located about halfway between the surface and the detector 100 m underground—and the detector in order to arrive at a constant gas flow into all detector sections. As Fig. 17 shows, the individual pressure regulation of the TRD sections works with high precision ($\sigma \approx 0.03$ mbar).

Membranes separate CO_2 from Xe, e.g. for filling the detector with Xe (while removing CO_2) and for

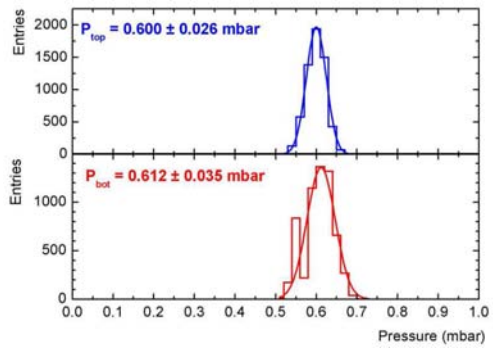

Figure 17: A realistic test of Xe-gas mixture distribution to two separate volumes 7 m apart in height and 40 m below the pump. In both cases a small overpressure of around 0.6 mbar was achieved with high precision.

emptying the Xe from the detector (then CO_2 is injected back into the loop) before sending it to the recovery. Oxygen is removed by copper catalyzers. In the cryogenic Xe recovery plant (reused from the ALEPH experiment) the Xe gas freezes, as it enters the plant. Then any Nitrogen present in the gas mixture is pumped out and the Xe is warmed up again and can be compressed into gas bottles.

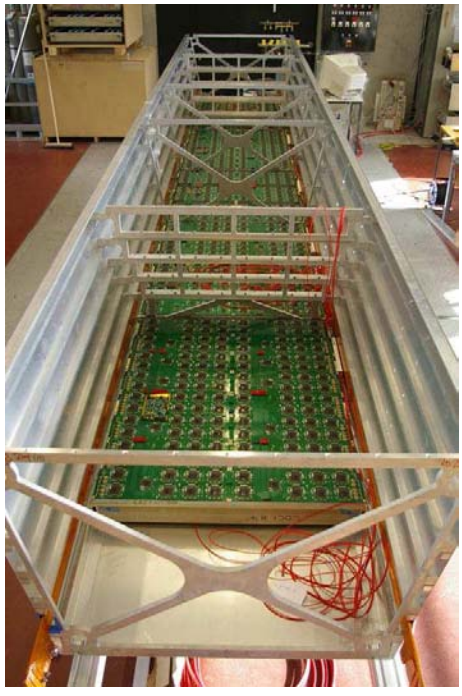

Figure 18: First TRD supermodule currently under construction. The lowest layer of TRD drift chambers with readout electronics is inserted. Five more layers will follow.

7. Summary & Outlook

The ALICE TRD is composed of large drift chambers with drift direction perpendicular to the wire planes. It implements 1.18 million analog channels, which are digitized during the 2 μs drift time. 65664 multi chip modules, each equipped with a preamplifier/shaper, an ADC, digital filters and a four-fold processor, perform on-detector integrated signal processing and store and forward the event data.

The TRD provides a pion rejection factor of 100 at (2 GeV/c), a stand-alone transverse momentum resolution below 4 % (around 1 GeV/c) and a fast trigger decision. To provide the trigger decision, all of the up to 16 000 charged particles have to be tracked online within 6 μs in order to find the stiff electron tracks.

The TRD gas system is designed to cope with the difficulties associated with the used heavy gas mixture (Xe, CO_2) and with the need to maintain small overpressure in the detectors.

For the first beam in summer 2007 four out of 18 supermodules are planned to be be ready. The first supermodule is currently constructed at the University of Heidelberg, Germany (See Fig. 18).

References

[1] ALICE, A Large Ion Collider Experiment at CERN, http://aliceinfo.cern.ch/

[2] The ALICE Collaboration, ALICE TRD Technical Design Report, *CERN/LHCC 2001-021*, ALICE TRD 9, 3 October 2001.

[3] A. Andronic et. al., Nucl. Instr. Meth. Phys. Res. A 525 (2004), 447; physics/0402043

[4] A. Andronic et. al., Nucl. Instr. Meth. Phys. Res. A 498 (2003), 143-154; physics/0303059

[5] A. Andronic et. al., Nucl. Instr. Meth. Phys. Res. A 519 (2004), 508; physics/0310122.

[6] C.W. Fabjan and W. Struczinski, Phys. Lett. B57 (1975), 483-486.

[7] A. Andronic et. al., Nucl. Instr. Meth. Phys. Res. A 558 (2006), 516-525; physics/0511229.

[8] A. Andronic et al., Nucl. Instrum. Meth. Phys. Res. A 522 (2004), 40; physics/0402131.

[9] C. Adler et. al., Nucl. Instr. Meth. Phys. Res. A 552 (2005), 364-371; physics/00506202.

[10] C. Adler et. al., Nucl. Instr. Meth. Phys. Res. A 540 (2004), 140-157; physics/0511233.

[11] J.P. Wessels et al., Frascati Phys. Ser. XXV (2001), 121-130.

[12] V. Angelov et al., Frascati Phys. Ser. XXV (2001), 135-139.

[13] F. Lesser, dissertation, Univ. of Heidelberg, Germany, 2002; HD-KIP-02-34.

[14] M. Gutfleisch, diploma thesis, Univ. of Heidelberg, Germany, 2002; HD-KIP-02-24.